Supplementary Materials for

Low-crystalline Tungsten Trioxide Anode with Superior Electrochemical Performance for Flexible Solid-state Asymmetry Supercapacitor

Jiayi Chen, Haiyan Wang, Jiang Deng, Chunmei Xu and Yong Wang**

This PDF file includes:

EXPERIEMNTAL

Assembly of the solid-state ASC: 4 g H_2SO_4 and 4 g PVA were mixed with 40 mL deionized water under continuously stirring. The whole mixture heated at 85° C until it became clear. The PVA-H_2SO_4 system was prepared as described above as gel electrolyte. LC-WO_3/TCC and TCC were served as the positive and negative electrodes, respectively. And then these two electrodes were placed face to face with area of 1 cm^2 by the filter paper filled with PVA-H_2SO_4 electrolyte. Finally, solid-state ASC was finished after an hour of drying and the thickness was ~0.90 mm including two electrodes, separator and electrolyte.

Calculation Methods

The following equations are used for calculating SCs performance:

Areal capacity (mF cm^{-2}), $$C_A = \frac{I \times t}{S \times \Delta V}$$

Volume capacity (mF cm^{-3}), $$C_V = \frac{I \times t}{V \times \Delta V}$$

Areal energy density (mW h cm^{-2}), $$E_A = \frac{C_A \times \Delta V^2}{2} \times \frac{1}{3600}$$

Volume energy density (mW h cm^{-3}), $$E_V = \frac{C_V \times \Delta V^2}{2} \times \frac{1}{3600}$$

Areal power density (mW cm^{-2}), $$P_A = \frac{E_A}{t}$$

Volume power density (mW cm^{-3}), $$P_V = \frac{E_V}{t}$$

Where I (A) is the current of discharge, t (s) is the discharge time, S represents the test area of electrode, ΔV (V) represents the voltage change of the test, and V (cm^{-3}) is the test volume of electrode.

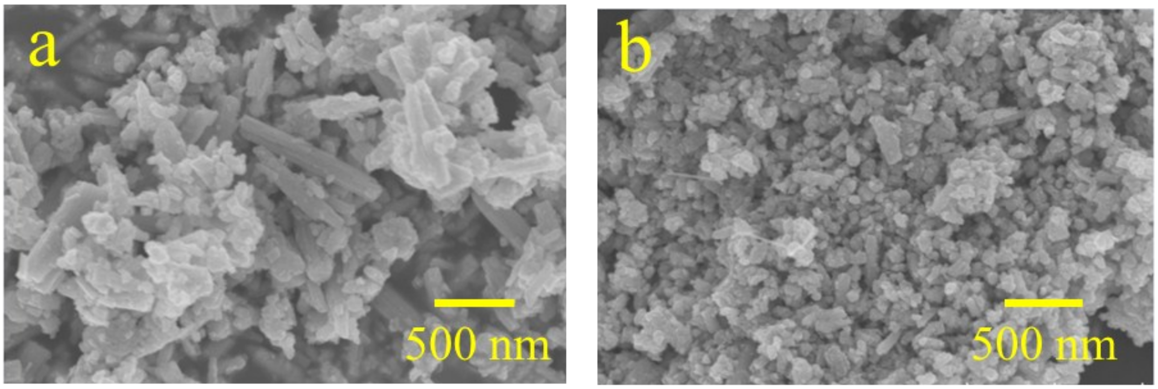

Figure S1. a) and b) SEM image of the HC-WO_3 and LC-WO_3, respectively.

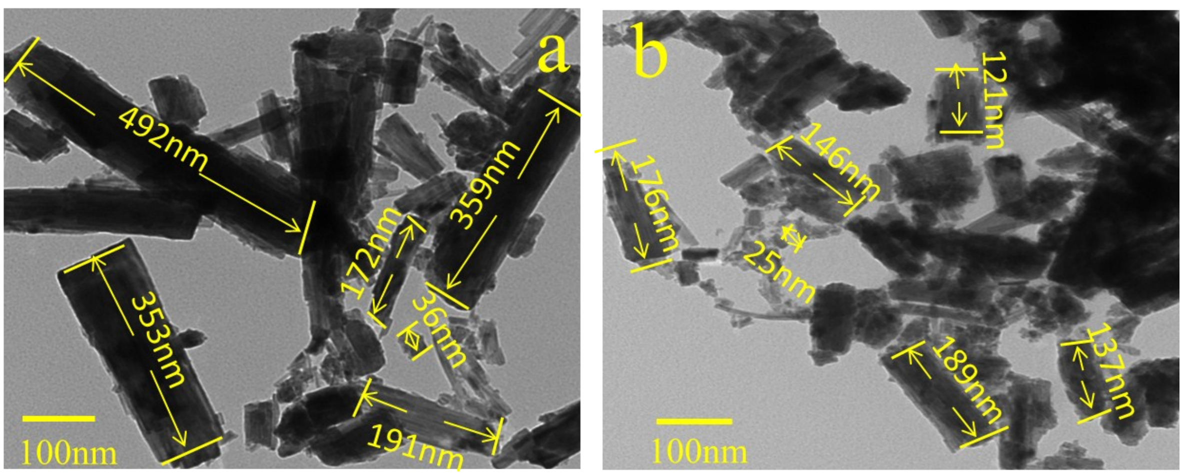

Figure S2. a) and b) TEM image of the HC-WO_3 and LC-WO_3, respectively.

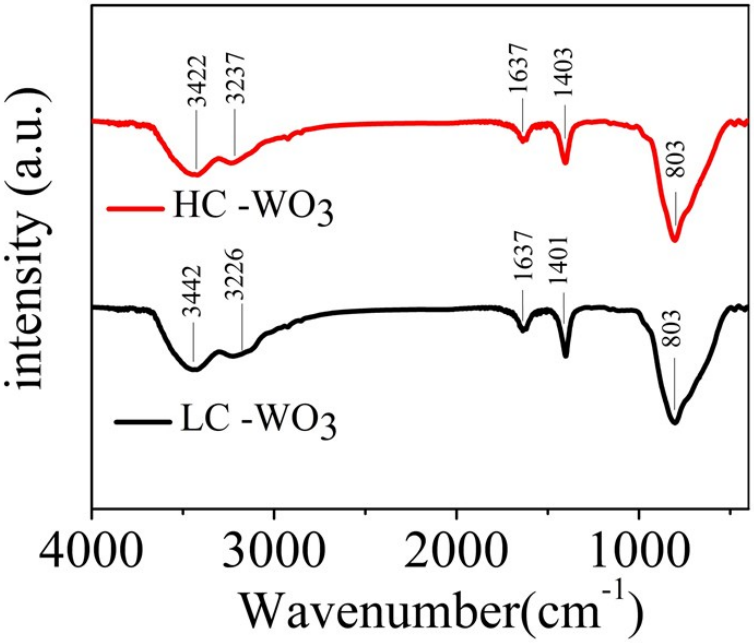

Figure S3 FTIR patterns of LC-WO_3 and HC-WO_3, respectively.

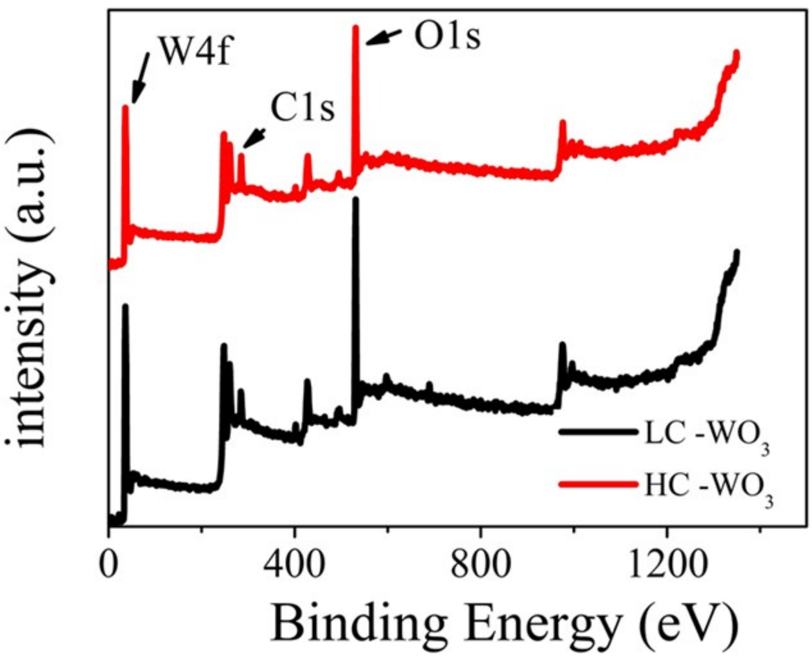

Figure S4. The XPS spectra of HC-WO_3 and LC-WO_3

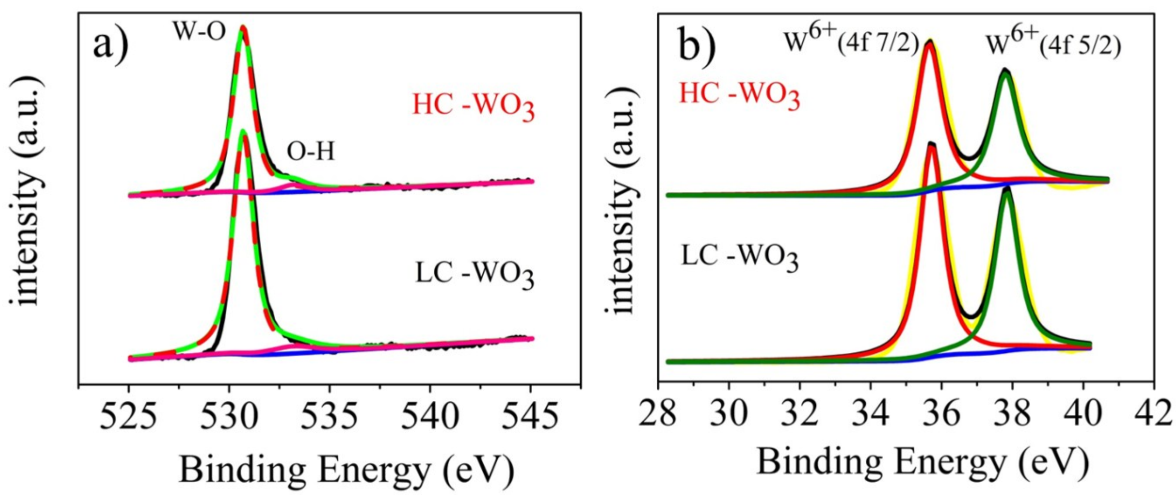

Figure S5. a) The O1s and b) W4f XPS fine scan spectrum of HC-WO_3 and LC-WO_3.

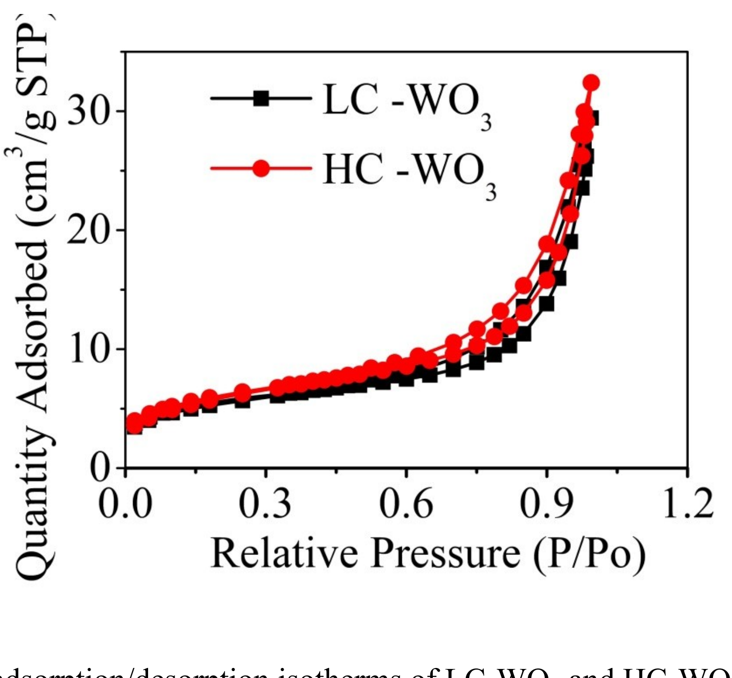

Figure S6. N_2 adsorption/desorption isotherms of LC-WO_3 and HC-WO_3.

Table S1. Porosity measurements of LC-WO_3 and HC-WO_3 using nitrogen adsorption/desorption tests.

Materials	**S_{BET}[a] (m^2 g^{-1})**	**Pore volume (cm^3 g^{-1})**			**Average pore width (nm)**
		V_{Total}[b]	**V_{Micro}[c]**	**V_{Micro}/V_{Total}**	
LC -WO_3	19	0.044	0.005	11%	8.3
HC -WO_3	21	0.050	0.005	10%	8.4

[a] Brunuaer–Emmett–Teller surface area; [b] Calculated by single-point adsorption; [c] Calculated by t-plot method.

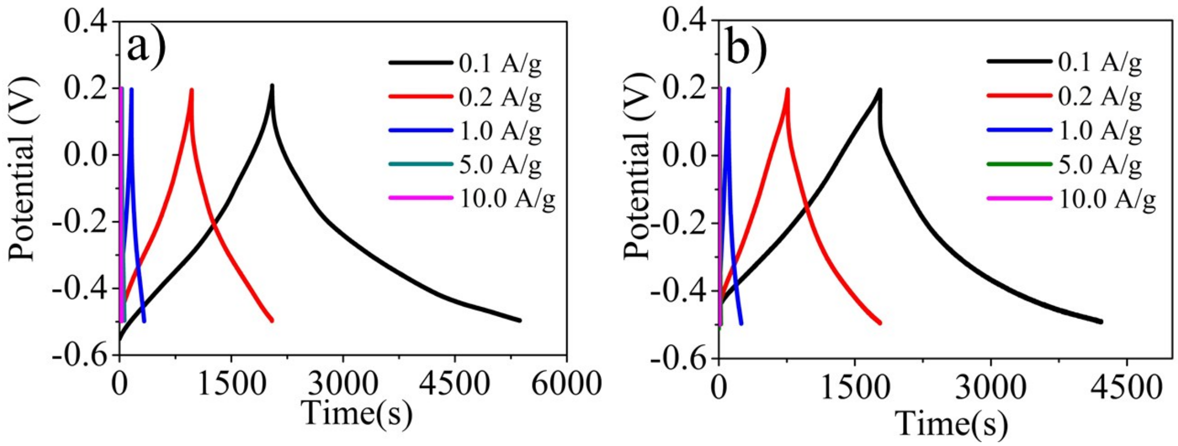

Figure S7. a) and b) GCD curves for LC-WO_3 and HC-WO_3, respectively.

.

Table S2. Resistance values of the LC-WO_3 and HC-WO_3 electrodes

Sample	Rs (Ω)	Rct (Ω)
HC-WO_3	0.17	1.5
LC-WO_3	0.27	0.9

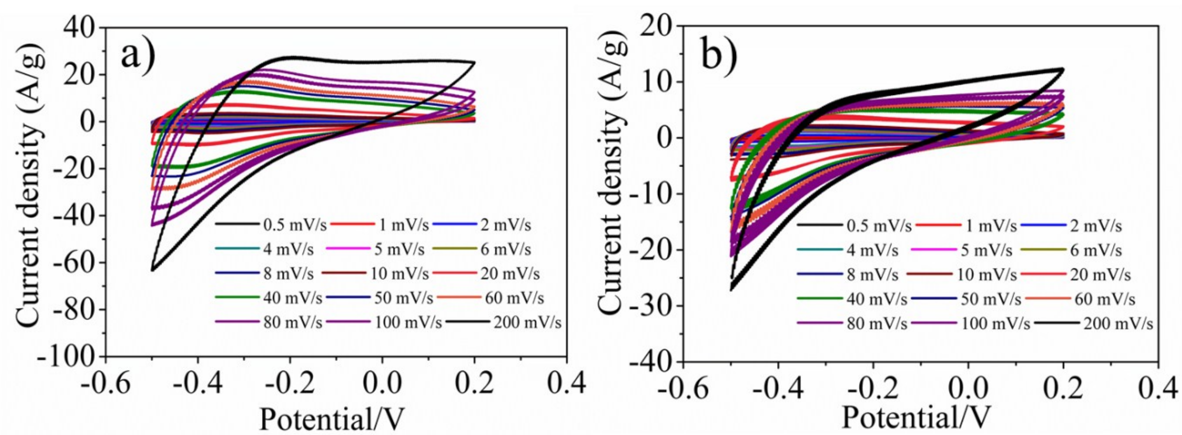

Figure S8. a) and b) CV curves of LC-WO_3 and HC-WO_3 at various scan rates, respectively.

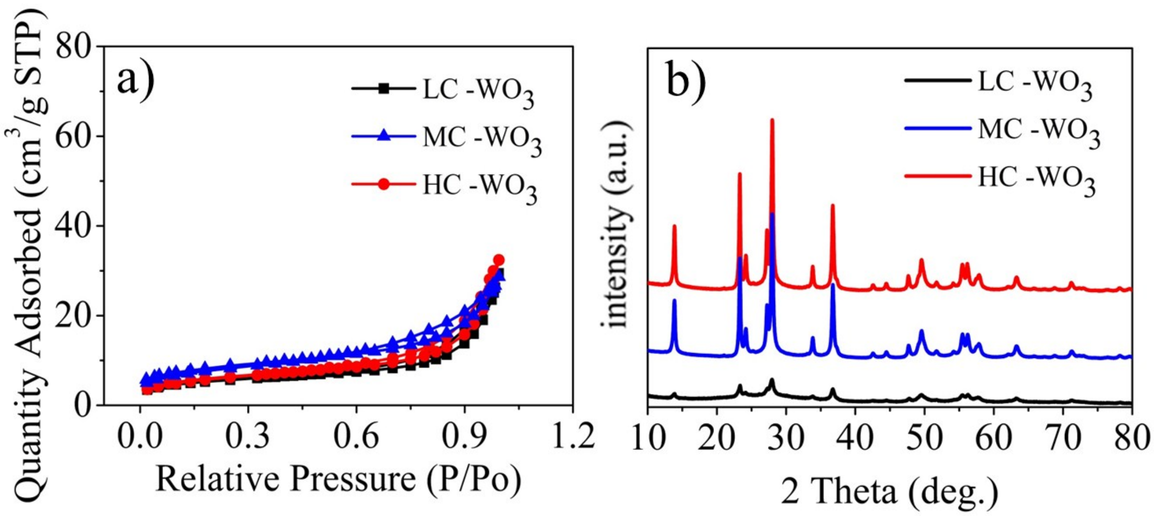

Figure S9 a) XRD patterns of LC-WO_3, MC-WO_3 and HC-WO_3, respectively. b) N2 adsorption/desorption isotherms of LC-WO_3, MC-WO_3 and HC-WO_3, respectively.

Table S3. Porosity measurements of MC-WO_3 using nitrogen adsorption/desorption tests.

Materials	**S_{BET}[a] (m^2 g^{-1})**	**Pore volume (cm^3 g^{-1})**			**Average pore width (nm)**
		V_{Total}[b]	**V_{Micro}[c]**	**V_{Micro}/V_{Total}**	
MC -WO_3	29	0.043	0.007	16%	6.0
[a] Brunuaer–Emmett–Teller surface area; [b] Calculated by single-point adsorption; [c] Calculated by t-plot method.					

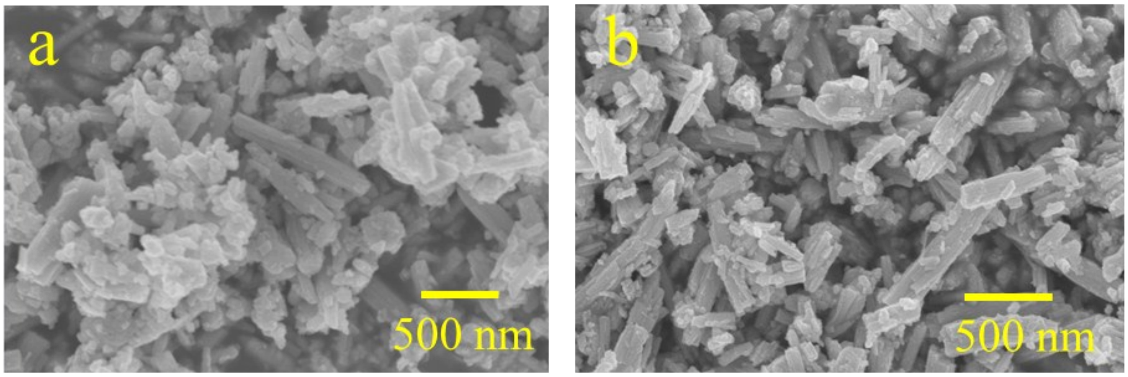

Figure S10. a) and b) SEM image of the HC-WO_3 and MC-WO_3, respectively.

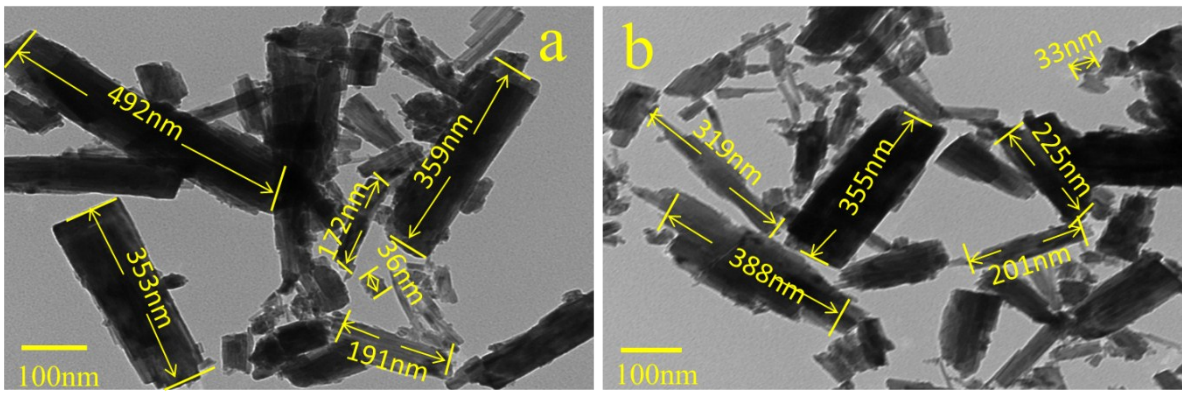

Figure S11. a) and b) TEM image of the HC-WO_3 and MC-WO_3, respectively.

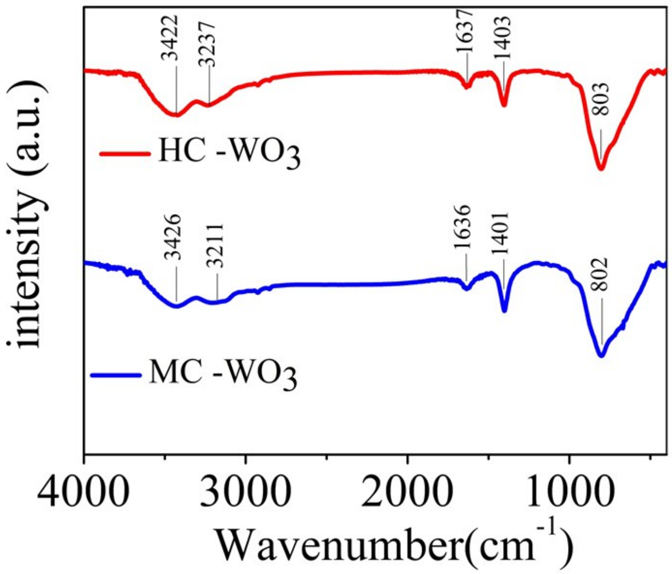

Figure S12 FTIR patterns of HC-WO_3 and MC-WO_3, respectively.

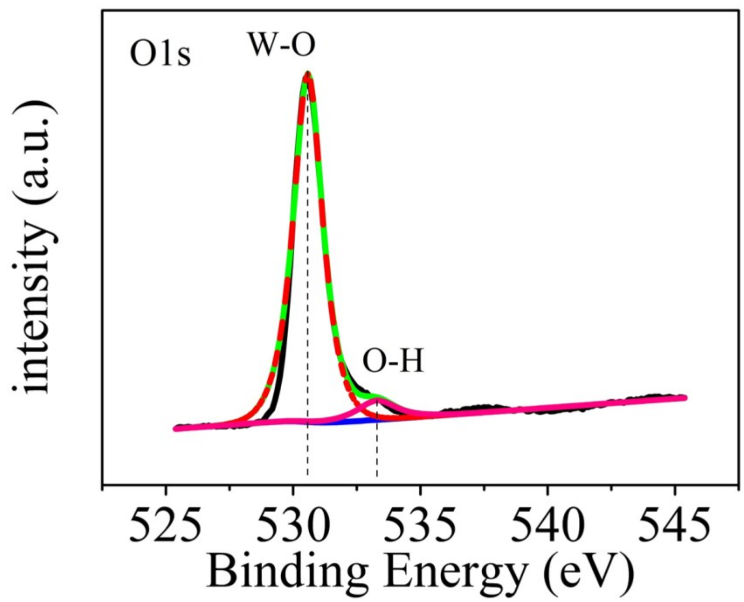

Figure S13. The O1s XPS fine scan spectrum of MC-WO_3

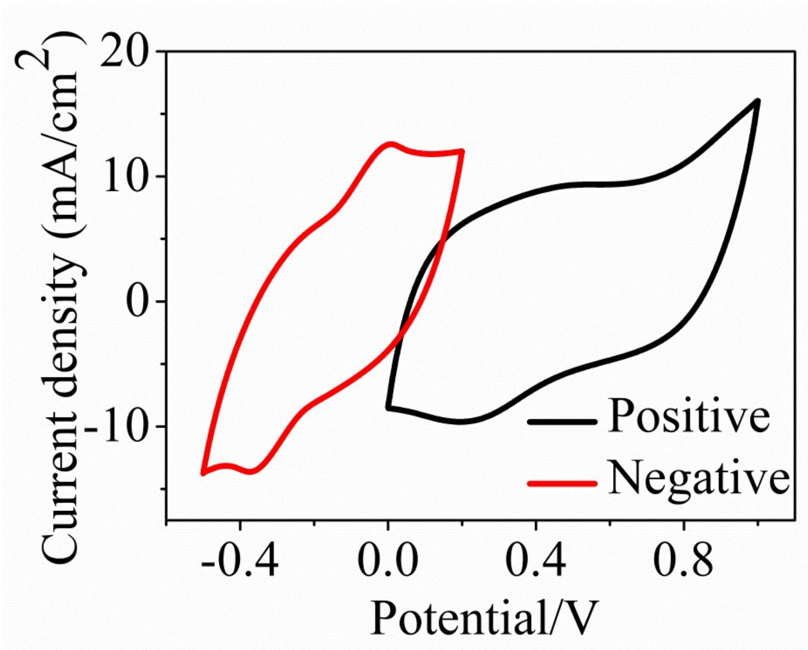

Figure S14. CV curves of negative and positive, respectively.

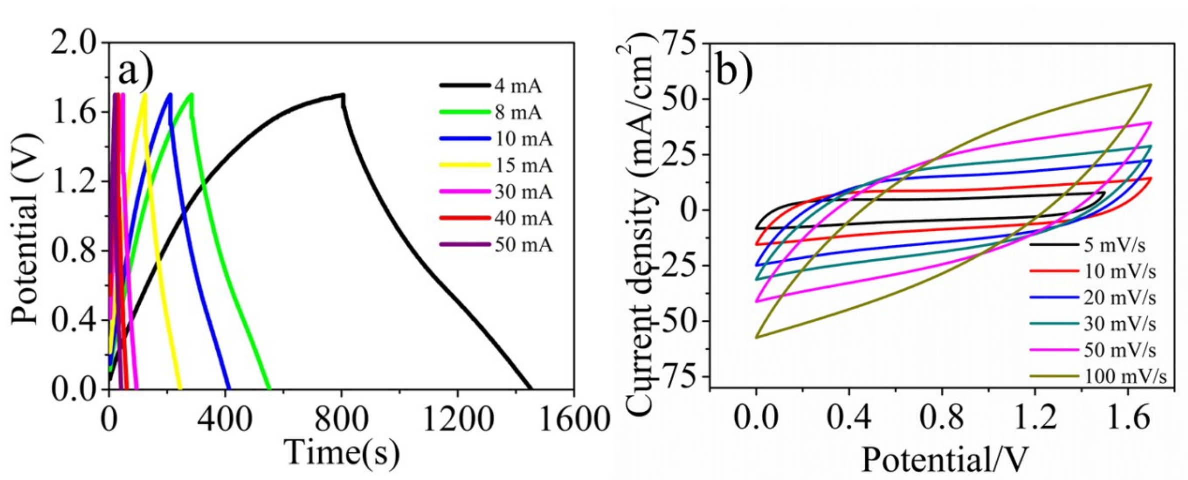

Figure S15. a) GCD curves for the solid-state flexible ACS device. b) CV curves for the solid-state flexible ACS device.

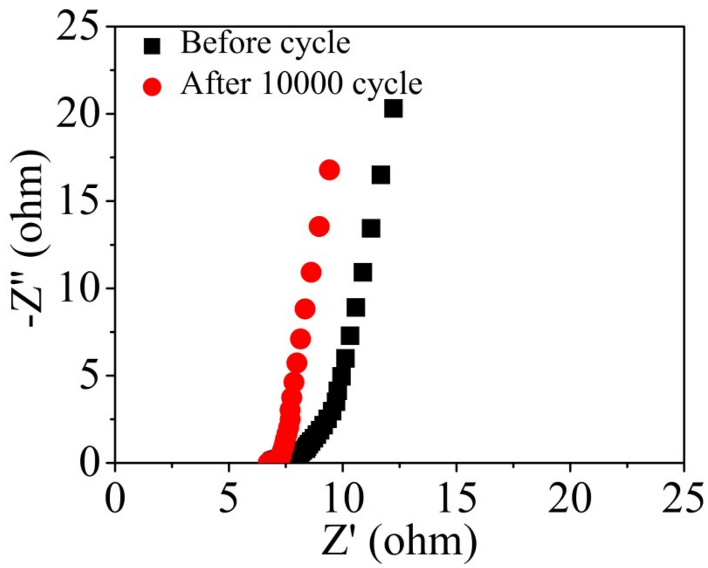

Figure S16. Nyquist plot of the device before and after cycling.

Table S4. Comparison of the electrochemical performance of solid-state TCC//LC-WO_3/TCC ASC in this work with other additives solid-state SCs reported in previous reports.

Devices	$C_{A, device}$ (mF/cm^2)	$C_{v, device}$ (F/cm^3)	$E_{A, stack}$ ($\mu Wh/cm^2$)	$E_{v, stack}$ (mWh/cm^3)
TCC//LC-WO_3/TCC, (this work)	1693	22.1	660	7.6
TCC//TCC, Ref.[1]	920	10.2	128	1.4
Bi_2O_3-CC//MnO_2-CC Ref.[2]	97	/	43.4	/
ACC//ACC Ref.[3]	31	0.36	4.3	0.05
WO_{3-x}/MoO_{3-x}//PANI/carbon fabric, Ref.4	216	/	/	1.9
NFL-WO_3//TiO_2@C@PPY Ref.[5]	658	/	/	0.53

Bamboo-likefibers//Bamboo-likefibers, Ref.[6]	/	2.1	/	0.24
PPy-coated paper Ref.[7]	420	11	37	1
PANI-ZIF-67-CC//PANI-ZIF-67-CC Ref.[8]	36	0.116	4.4	0.0161
NCTs/ANPDM//Fe_2O_3 Ref.[9]	/	0.131	/	0.097
Co_9S_8//Co_3O_4@RuO_2 on CC Ref.[10]	/	4.28	/	1.44
MnO_2@TiN-ACC//EACC-10 Ref.[11]	/	2.69	/	1.5

REFERENCES

1. Wang, H.; Deng, J.; Xu, C.; Chen, Y.; Xu, F.; Wang, J.; Wang, Y., Ultramicroporous carbon cloth for flexible energy storage with high areal capacitance. Energy Storage Mater. 2017, 7, 216-221.

2. Xu, H.; Hu, X.; Yang, H.; Sun, Y.; Hu, C.; Huang, Y., Flexible Asymmetric Micro-Supercapacitors Based on Bi_2O_3 and MnO_2 Nanoflowers: Larger Areal Mass Promises Higher Energy Density. Adv. Energy Mater. 2015, 5,.

3. Wang, X.; Lu, X.; Liu, B.; Chen, D.; Tong, Y.; Shen, G., Flexible Energy-Storage Devices: Design Consideration and Recent Progress. Adv. Mater. 2014, 26, 4763-4782.

4. Xiao, X.; Ding, T.; Yuan, L.; Shen, Y.; Zhong, Q.; Zhang, X.; Cao, Y.; Hu, B.; Zhai, T.; Gong, L.; Chen, J.; Tong, Y.; Zhou, J.; Wang, Z. L., WO_{3-x}/MoO_{3-x} Core/Shell Nanowires on Carbon Fabric as an Anode for All-Solid-State Asymmetric Supercapacitors. Adv. Energy Mater. 2012, 2, 1328-1332.

5. Qiu, M.; Sun, P.; Shen, L.; Wang, K.; Song, S.; Yu, X.; Tan, S.; Zhao, C.; Mai, W., WO_3 nanoflowers with excellent pseudo-capacitive performance and the capacitance contribution analysis. J. Mater. Chem. A 2016, 4, 7266-7273.

6. Sun, Y.; Sills, R. B.; Hu, X.; Seh, Z. W.; Xiao, X.; Xu, H.; Luo, W.; Jin, H.; Xin, Y.; Li, T.; Zhang, Z.; Zhou, J.; Cai, W.; Huang, Y.; Cui, Y., A Bamboo-Inspired Nanostructure Design for Flexible, Foldable, and Twistable Energy Storage Devices. Nano Letters 2015, 15, 3899-3906.

7. Yuan, L.; Yao, B.; Hu, B.; Huo, K.; Chen, W.; Zhou, J., Polypyrrole-coated paper for flexible solid-state energy storage. Energ.Environ. Sci. 2013, 6, 470-476.

8. Wang, L.; Feng, X.; Ren, L.; Piao, Q.; Zhong, J.; Wang, Y.; Li, H.; Chen, Y.; Wang, B., Flexible Solid-State Supercapacitor Based on a Metal–Organic Framework Interwoven by Electrochemically-Deposited PANI. J. Am. Chem. Soc. 2015, 137, 4920-4923.

9. Lv, Q.; Wang, S.; Sun, H.; Luo, J.; Xiao, J.; Xiao, J.; Xiao, F.; Wang, S., Solid-State Thin-Film Supercapacitors with Ultrafast Charge/Discharge Based on N-Doped-Carbon-Tubes/Au-Nanoparticles-Doped-MnO2 Nanocomposites. Nano Letters 2016, 16, 40-47.

10. Xu, J.; Wang, Q.; Wang, X.; Xiang, Q.; Liang, B.; Chen, D.; Shen, G., Flexible Asymmetric Supercapacitors Based upon Co9S8 Nanorod//Co_3O_4@RuO_2 Nanosheet Arrays on Carbon Cloth. ACS Nano 2013, 7, 5453-5462.

11. Wang, W.; Liu, W.; Zeng, Y.; Han, Y.; Yu, M.; Lu, X.; Tong, Y., A Novel Exfoliation Strategy to Significantly Boost the Energy Storage Capability of Commercial Carbon Cloth. Adv. Mater. 2015, 27, 3572-3578.